New Journal of Physics
The open access journal for physics

Acoustic whispering-gallery modes in optomechanical shells

Gaurav Bahl[1,4], **Xudong Fan**[2] **and Tal Carmon**[3]

[1] Mechanical Science and Engineering, University of Illinois at Urbana-Champaign, Urbana, IL, USA
[2] Biomedical Engineering, University of Michigan at Ann Arbor, Ann Arbor, MI, USA
[3] Electrical Engineering and Computer Science, University of Michigan at Ann Arbor, Ann Arbor, MI, USA
E-mail: bahl@illinois.edu

New Journal of Physics **14** (2012) 115026 (14pp)
Received 18 May 2012
Published 27 November 2012
Online at http://www.njp.org/
doi:10.1088/1367-2630/14/11/115026

Abstract. We numerically calculate the forms and frequencies of mechanical whispering-gallery modes in silica shells. Such modes were recently experimentally observed in water-filled optomechanical resonators, which constitute a bridge between optomechanics and microfluidics. We consider the three acoustic mode families of Rayleigh–Lamb waves, longitudinal waves and Love waves. Our study shows that these acoustic modes have rich velocity dispersion characteristics and can create considerable deformation of the inner surface of the shells. In this manner, a novel optomechanical interaction may be facilitated between fluids and light.

S Online supplementary data available from stacks.iop.org/NJP/14/115026/mmedia

[4] Author to whom any correspondence should be addressed.

Contents

1. Introduction

Optomechanical oscillators [1–13] present an alternative to electrode-based mechanical actuation methods. More specifically, in Brillouin optomechanics two optical beams can interfere to write a train of virtual electrodes at regular separation and at high spatial and temporal frequencies, which unlike metal contacts are immune to electrical impedance. Electrostriction, which is common to all dielectrics, can then convert this field to an actuation force. This mechanism is generally referred to as Brillouin scattering [14, 15] and has rarely been used as an actuation mechanism in microdevices. Recently, Brillouin scattering was shown to actuate mechanical vibration in silica microshells filled with water [16]. Here, we theoretically analyze the modal structure and frequency of the acoustic modes in silica shells using finite element calculation, revealing a considerable penetration of deformation into the internal space where fluids may flow.

1.1. Brillouin mechanism for optomechanical actuation and cooling

Stimulated Brillouin scattering (SBS) [14, 15] has been for many years considered as an optical gain mechanism for lasers [17] and as a tool for optical phase conjugation [18], slow light [19], non-destructive characterization of materials [20–22] and optical gyroscopes [23]. It is notable that SBS has an optical nonlinearity that is common to all dielectrics in any state of matter. In many fiber-based communication systems SBS is often considered as an undesirable interfering mechanism [24]. In addition to optical fibers and bulk materials, SBS has been demonstrated in fluid droplets [25], nano-spheres [26], photonic-crystal fibers [27], millimeter-scale crystalline resonators [28] and in microspheres [29]. In all these examples, light backscatters from hypersound in the material, resulting in a red-shifted (Stokes) optical signal. In the process, light imparts energy to the acoustic wave and amplifies it. The phase-matching requirements for SBS specify that the optical modes need to be separated by the energy and

momentum of the acoustic mode. As a result, for backscattered SBS, the accessible acoustic frequencies are constrained to be in the 10 GHz regime. In nanoscale resonators [26] this process was deterred by zero optical finesse, whereas in larger resonators [28, 29] the mechanical finesse was seen to be very low. Simultaneous resonant enhancement of the optical and acoustic modes is important as it improves the Brillouin interaction in these systems.

It was proposed recently [30] that reversing the scattering direction from backwards [17] to forwards [27, 30, 31] would allow access to acoustic whispering-gallery modes (WGMs) at low frequencies and high mechanical quality factor. Indeed, reversing the scattering direction to forwards experimentally enabled vibration at hundreds of MHz in amorphous silica microspheres [32] and in crystalline ($LiTaO_3$ and MgF_2) resonators [33]. These low-frequency acoustic modes were shown to have long phonon lifetimes, up to two orders of magnitude longer than the photon lifetimes in these high-Q devices [32, 34]. This lengthened phonon lifetime was in accordance with what is needed for cooling [35], as a result of which spontaneous Brillouin cooling was experimentally observed [34, 36]. To summarize, Brillouin scattering can excite mechanical WGMs at vibrational rates from tens of MHz [16, 32, 33] to tens of GHz [28, 29]. In addition, the direction of energy transfer in the Brillouin process can be reversed to support the cooling of microdevices [34].

The Brillouin optomechanical process involves two optical modes that are separated by the acoustic resonance frequency. These optical modes can be obtained either by designing the free spectral range (FSR) of the resonator or by exploiting aperiodic spacing between high transverse order optical modes in a resonator [32, 37, 38]. Aperiodic spacing between resonances is particularly helpful in suppressing scattering in the Stokes direction when only anti-Stokes scattering is desired. This selective filtering capability was also exploited to achieve spontaneous Brillouin cooling of the acoustic WGMs [34, 36].

1.2. Optomechanics in fluidic systems

Optofluidic devices [39] have been employed as extremely sensitive label-free detectors [40, 41] for single nanoparticles [42, 43] and viruses [44, 45] in fluid media and also for vapor identification [46]. These sensors operate on the concepts of optical mode splitting [42] and optical mode shifts [43, 45, 46], and have also been functionalized with polymers for gas detection [46, 47].

Prior to recent results [16, 48], optomechanical actuation had not been demonstrated in the presence of fluids. This is because in liquid-submerged optomechanical devices, acoustic radiative losses increase on account of the acoustic impedance of liquids being much larger than that of air. In addition to overcoming the challenge associated with radiative acoustic losses, these capillary-based systems also provide solutions for delivering small volumes of analyte to the 'active' sensing region of the device. Furthermore, optically opaque fluids can also be used in these capillary based devices as the optical modes can be kept in the silica while coupled acoustic vibrations extend into the liquid.

In these studies [16, 48], the authors fabricated hollow microfluidic optomechanical resonators with fused silica glass, starting from a seed capillary [49]. The capillaries were heated using CO_2 lasers to soften the glass, and pulled lengthwise at a constant rate. Modulation of the laser power changed the heating of the silica glass, resulting in a modulation of the capillary radius. In the region of greatest radius (*the equator*), these devices can confine light effectively, thereby forming a whispering-gallery optical microresonator. The geometry of these devices is

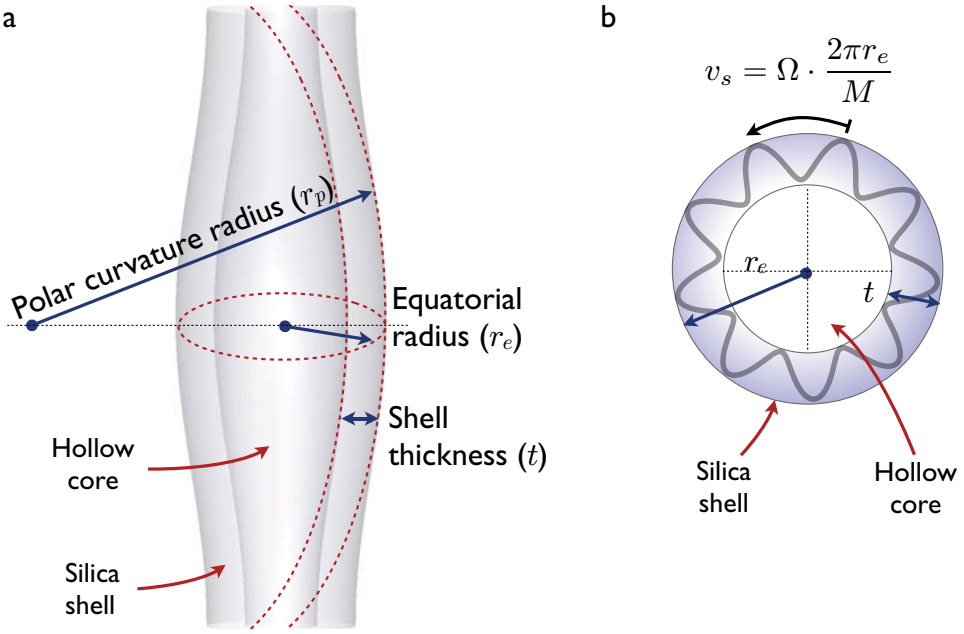

Figure 1. Illustration of the main dimensions of the optomechanical resonator. Numerical calculations in this paper consider a hollow silica shell resonator with air inside. (a) The optical and acoustic modes are confined at the equator, illustrated by the dashed circle and radius parameter r_e. (b) The equatorial cross-section is portrayed along with a sinusoidal representation of the acoustic wave of azimuthal order $M = 9$. The acoustic velocity v_s is defined at the surface of the resonator. Ω represents the acoustic frequency.

illustrated in figure 1. Light can be coupled evanescently to the optical WGMs using a suitable tapered optical waveguide (optical fiber) [50, 51].

Acoustic WGMs are confined at the equator in a manner similar to the optical modes. Since the optical WGMs and acoustic WGMs have considerable overlap in this region, an optomechanical Brillouin process is supported that can be used to excite [32] or cool [34] the acoustic modes. Experimentally, mechanical WGMs at frequencies ranging from 99 MHz to 11 GHz [16] were excited in a single hollow device filled with water, using only 160 μW of input optical power, representing the first bridge between microfluidic systems and optomechanical systems. These devices have optical quality factor in the range of 10^8, and no quality factor degradation was observed when filled with water-based liquids. This is because the optical mode is confined to the outer periphery of the device (only a few microns deep), while the liquid is located much deeper inside where it cannot affect the optical properties of the silica.

While the numerical solutions to optical WGMs in such capillaries are available [52], their mechanical WGMs [53] have not been analyzed. This paper discusses the form and frequency dispersion properties of the acoustic WGMs that interact with optical WGMs via the Brillouin mechanism in such shell-type optomechanical resonators.

2. Acoustic whispering-gallery modes (WGMs) in shell resonators

2.1. Dimensional and wave-description variables

We define three-dimensional parameters of the capillary-type optomechanical resonators near the equatorial region where both optical and acoustic modes are confined. r_p is the radius of curvature in the polar (or longitudinal) direction. r_e is the radius of the capillary at the equator where the modes are confined. t is the thickness of the resonator walls. These three parameters are illustrated in figure 1.

In the interest of further constraining the free parameters for numerical calculations, we select a fixed $r_p = 1500\,\mu$m and $r_e = 50\,\mu$m corresponding to the type of capillary in which we have found it easy to experimentally excite the mechanical WGMs. Our studies indicate that modifying the r_p parameter does not significantly perturb the calculated forms and frequencies of the acoustic modes.

Similar to the manner in which optical WGMs are represented, we define an integer momentum parameter M for the acoustic WGMs in the device, which relates to azimuthal propagation $e^{i(M\phi-\Omega t)}$ around the device equator. Here ϕ is the azimuthal angular position, and Ω is the mechanical frequency. M is therefore equal to the number of acoustic wavelengths around the circumference of the device.

At high M numbers the acoustic waves do not experience the curvature of the device, resulting in acoustic velocities that asymptotically converge to the value on planar surfaces. At low M numbers the acoustic waves are strongly affected by the equatorial curvature of the device, and the acoustic velocity is therefore modified.

Furthermore, by defining a ratio of shell thickness to the equatorial radius as $R = t/r_e$, we can generalize the acoustic velocity solution for a given R independent of scaling.

2.2. Notes on numerical calculations

The mechanical WGMs described in this paper were numerically solved using eigenfrequency analysis with COMSOL Multiphysics (Comsol Group, COMSOL Multiphysics). Fused silica glass was chosen as the shell material. We chose not to include a fluid in our numerical calculations since the interaction with an enclosed fluid is a secondary effect. That is to say, light primarily interacts with the solid material of the optical resonator, and the mechanical mode subsequently interacts with the fluid. The presence of a fluid primarily adds dissipation to the mechanical mode and shifts the mechanical frequency by means of its viscosity and density, and is therefore specific to the chosen fluid.

The acoustic phase velocity at the surface is calculated in the manner described in figure 1(b) via the equation

$$v_s = \Omega \frac{2\pi r_e}{M}. \tag{1}$$

For each numerical calculation, the solved mechanical eigenfrequency Ω and the known momentum parameter M provide us with v_s.

2.3. Three types of mechanical WGMs in optomechanical shells

We investigate three types of acoustic WGMs (illustrated in figure 2) in the shell system, which are defined by the form of the acoustic waves that compose them. Visualizations of all three

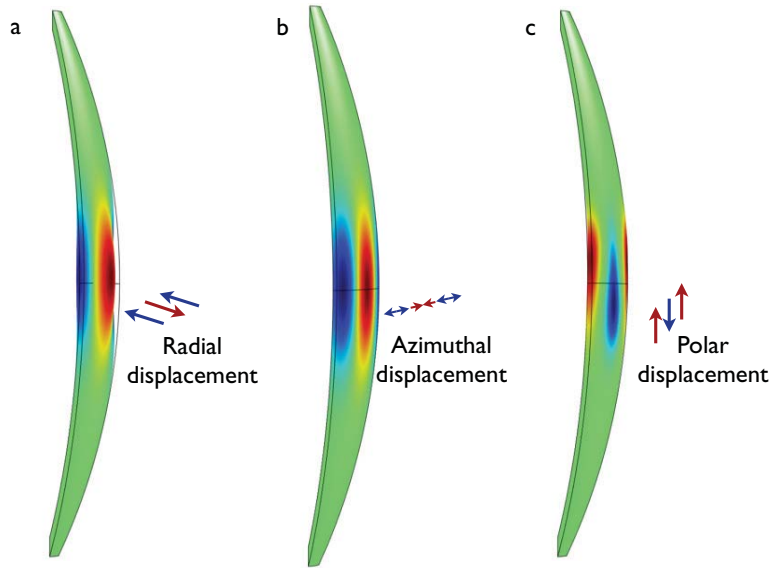

Figure 2. The three mode families discussed in this paper are comprised of (a) Rayleigh–Lamb waves where particle motion is elliptical, (b) longitudinal waves where motion is in the azimuthal direction along the equator and (c) transverse (Love) waves where motion is in the polar direction. The calculated modes here have azimuthal parameters of $M = 8$, which is typically seen in experiments with such devices. Colors indicate radial displacement for Rayleigh modes, polar displacement for transverse modes, and azimuthal displacement for longitudinal modes, respectively (red is positive, blue is negative, and green is zero). Animated visualizations for the three mode families are available in the supplementary videos provided with this paper (available from stacks.iop.org/NJP/14/115026/mmedia).

mode families are provided in the animations that accompany this paper.

1. **Rayleigh–Lamb modes** comprised of Rayleigh waves (for large R) and Lamb waves (for small R), where the displacement trajectory of a fixed point on the resonator is elliptical.
2. **Longitudinal modes** comprised of longitudinal compression waves in the material, where the major component of deformation is along the azimuthal direction.
3. **Transverse (Love) modes** comprised of shear waves where the major component of deformation is transverse to wave propagation, in the polar direction.

For simplicity, we only discuss acoustic modes with one maximum along the plane transverse to propagation (i.e. first-order modes). All three families of modes create a photoelastic refractive index change along the equator, resulting in an index grating that light can scatter from. As these modes travel at their respective speeds of sound, the scattered light experiences a Doppler shift, according to the theory of Brillouin light scattering.

In solid spheres [53], all three mode families follow a similar trend, i.e. the acoustic phase velocity at the surface increases at low M numbers. In optomechanical shells, however, the velocity dispersion characteristics are far more interesting.

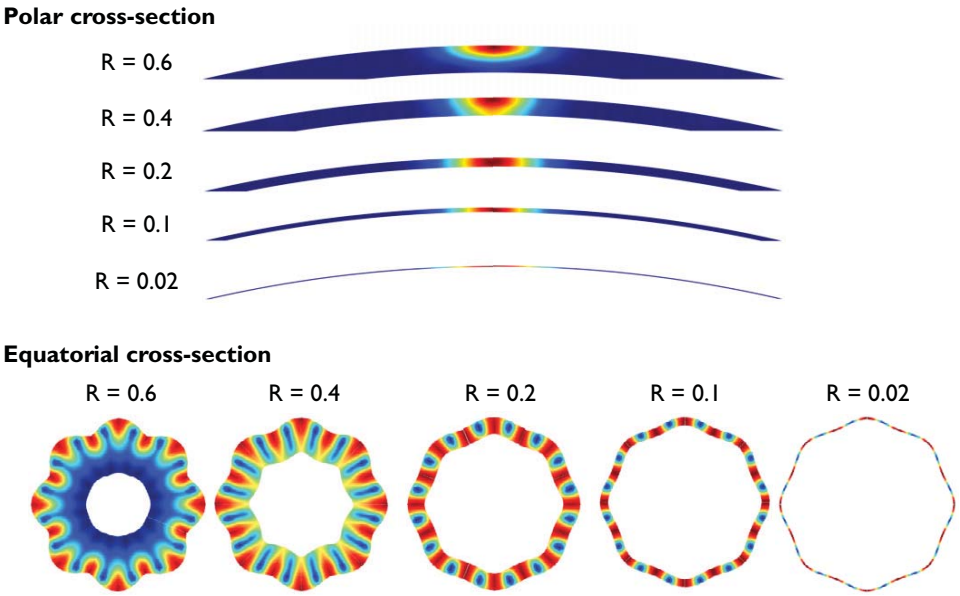

Figure 3. The form of the Rayleigh–Lamb waves. The modes are illustrated for various shell thicknesses t ranging from 1 to 30 μm ($R = t/r_e$ ranging from 0.02 to 0.6 since $r_e = 50\,\mu$m). The $M = 8$ modes are calculated here. Colors indicate the magnitude of displacement of the material (red is the maximum and blue is zero) and are normalized for each individual mode shape.

2.4. Acoustic velocity dispersion in the Rayleigh–Lamb modes

We numerically solve the Rayleigh–Lamb modes on optomechanical shells as a function of the azimuthal propagation constant M for various shell thicknesses t. Only WGMs with one maximum along the plane transverse to propagation, i.e. first-order modes, are considered. The numerical results for the $M = 8$ Rayleigh–Lamb waves are illustrated in figure 3. For thick shells, the wave solutions are similar to the Rayleigh wave solutions for solid spheres [53] since the surface wave is confined to the external surface of the resonator and does not encounter the inner free surface. When the shell thickness t is small (or equivalently R is low), the acoustic wave begins to travel on both surfaces of the shell, thereby taking the form of an anti-symmetric flexural-mode Lamb wave (figure 3). As a rule of thumb this change occurs when the acoustic wavelength is of the order of the shell thickness, which is to say that

$$t \approx \frac{2\pi r_e}{M}, \quad \text{or alternatively,} \quad R \approx \frac{2\pi}{M}. \tag{2}$$

The transition to the Lamb-wave regime brings about a reduction of acoustic velocity as seen in figure 4 since the wave now interacts with two free surfaces. It can be seen from figure 4 that the acoustic velocity for a very thin shell of $R = 0.02$ (i.e. $t = 1\,\mu$m for $r_e = 50\,\mu$m) can be as low as 140 m s^{-1} for $M = 4$.

In the intermediate regime, the acoustic phase velocity can rise above the Rayleigh wave velocity on planar surfaces (3410 m s^{-1}) just as it does on solid spheres [53]. This is because the

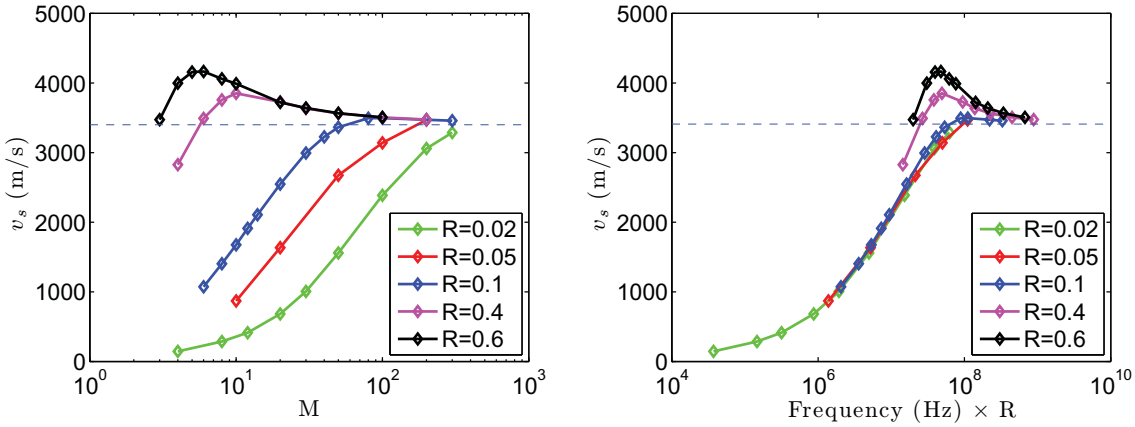

Figure 4. Velocity dispersion for the Rayleigh–Lamb waves calculated as a function of M and the frequency–thickness product. At high M, all dispersion curves approach the Rayleigh wave velocity on semi-infinite planar substrates, i.e. 3410 m s^{-1}, as indicated by the dashed line. At low M, the stiffness and acoustic velocity on the shell drop sharply since the acoustic wavelength is comparable to the shell thickness t.

curvature of the device is more significant at low M, which 'pushes' the wave deeper inside the device, reducing its exposure to the free surface and thereby increasing the material stiffness. The resulting increase in frequency appears as an increased acoustic phase velocity at the surface of the device.

2.5. Acoustic velocity dispersion in longitudinal modes

In contrast with bulk media, where longitudinal waves are not surface acoustic waves, the curvature of the surface here results in their confinement near the interface [29, 53] forming a longitudinal surface wave.

In solid spheres, at low M numbers the curvature of the device forces these waves deeper inside the material, thereby increasing the effective acoustic velocity [53]. Here, in the shell geometry, the waves exhibit interesting behavior in their velocity dispersion as a function of shell thickness. The numerically calculated acoustic velocities for first-order longitudinal waves are shown in figure 5. In this calculation, the thickness of the shell t (and hence R) is varied for fixed azimuthal modal orders M of the acoustic mode.

The reason for this odd trend in acoustic wave velocity can be explained with the help of figure 6 where the mode shapes are illustrated for $M = 8$. We see that for very small $R \leqslant 0.2$, the shell is thin enough such that the longitudinal acoustic wave travels on both surfaces simultaneously. In an intermediate region defined by $0.2 < R < 0.6$, where the shell thickness is comparable to the radial depth of the acoustic mode, there is significant anti-phase deformation of the inner free surface of the shell. This new mode shape is similar to an anti-symmetric (A_1) Lamb wave on a plate, which is slower and results in a sharp drop in the acoustic velocity. Finally, for thicker shells when $R \geqslant 0.6$, the acoustic wave is free of the inner surface and the acoustic velocity rises again. As seen in figure 5, the dip in velocity v_s occurs at lower values

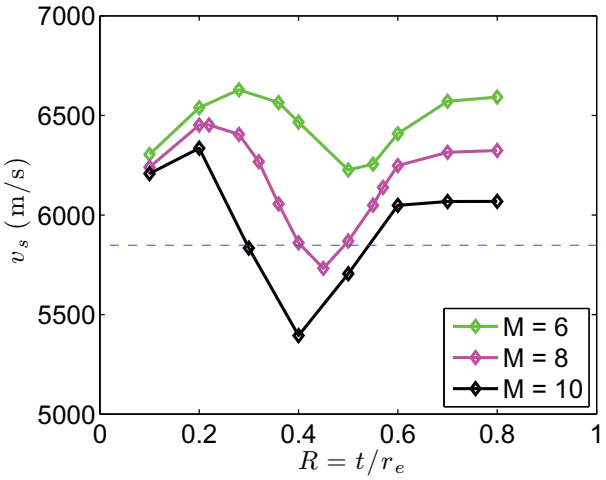

Figure 5. Velocity dispersion for longitudinal waves. The dashed line indicates the longitudinal wave velocity in bulk materials, i.e. 5848 m s^{-1}. The dip in the acoustic velocity curve for intermediate R numbers is due to the acoustic wave being shared by two surfaces, and is explained with the help of figure 6.

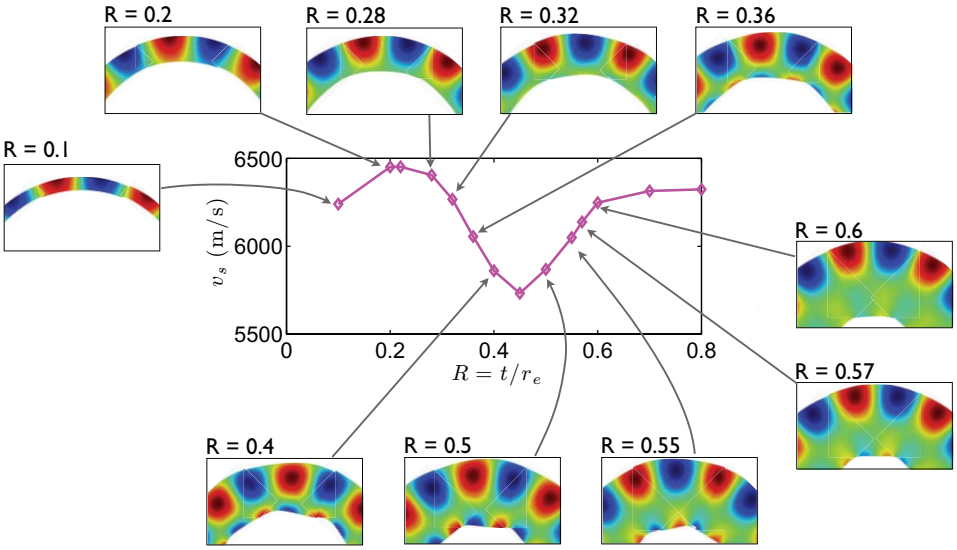

Figure 6. Equatorial cross-sections for longitudinal modes of $M = 8$. Colors represent azimuthal displacement (red is positive, blue is negative and green is zero). The seemingly anomalous dip in the acoustic velocity occurs in the case when the acoustic wave travels on both the inner and outer surfaces of the shell simultaneously. This resembles an anti-symmetric A_1 Lamb wave, which has a lower velocity.

of R for higher M numbers since the acoustic wavelength is shorter. In contrast with the case of solid spheres [53] the longitudinal WGMs that arise in shells do obtain v_s lower than their velocity in bulk materials (5848 m s^{-1}) as seen in figure 5.

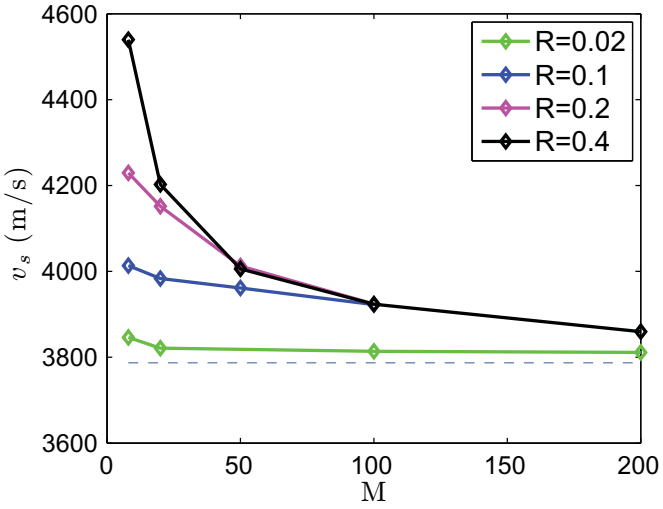

Figure 7. Velocity dispersion for the Love modes. At high M, the velocities for all cases approach the Love wave velocity on semi-infinite planar substrates, i.e. 3787 m s^{-1}, as indicated by the dashed line. At low M, the acoustic wave is pushed deeper inside the resonator, resulting in an increased acoustic phase velocity at the surface.

2.6. Acoustic velocity dispersion in transverse (Love) modes

The numerically calculated acoustic velocity dispersion for first-order Love waves is shown in figure 7. In this calculation, only the azimuthal mode order M is varied for various fixed thicknesses t of the shell.

At high M numbers, where curvature is not a significant perturbing factor, the Love waves approach their standard acoustic velocity on semi-infinite planar surfaces (3787 m s^{-1}).

At low M numbers, azimuthal curvature forces the waves to propagate radially deeper in the shell, resulting in an increase in the acoustic phase velocity at the surface. For thick shells (large R) this behavior is similar to solid spheres [53]. For thin shells, the Love wave velocity does not change much as there is no material deeper inside the resonator.

In contrast with the longitudinal modes and the Rayleigh–Lamb modes, the acoustic velocity for Love modes never drops below their acoustic velocity on semi-infinite planar surfaces.

2.7. Optomechanical coupling

It is important to quantify the optomechanical coupling strength of these shell-type resonators. It should be noted, however, that the conventional description of optomechanical coupling coefficient $g_0 = \mathrm{d}\omega/\mathrm{d}x$ cannot be applied here since the optical modes are not perturbed by the mechanical mode. The optomechanical coupling strength for a Brillouin optomechanical system was described in [54], and in the supplement to [34] it was shown that the formulation can be simplified to

$$g_0 = \left(\frac{\pi \gamma_e}{2\epsilon_r}\right) \cdot M \cdot \frac{\omega_{\text{optical}} \cdot \sqrt{\hbar}}{L \cdot \sqrt{2 \cdot m_{\text{eff}} \cdot \Omega}}, \tag{3}$$

where L is the effective equatorial circumference, γ_e is the electrostrictive coefficient for the host material, M is the momentum parameter described earlier, Ω is the acoustic frequency and m_{eff} is the effective mass of the mode. Our calculations in this study show that on thin shells there is a significant reduction in the effective mass of the acoustic mode as well as its acoustic frequency, which would result in a magnified optomechanical coupling strength compared with previously demonstrated solid devices [32–34].

3. Conclusions

Hollow [55–57] optomechanical shell resonators provide a novel platform for optomechanics with materials in their non-solid phases. In this paper, we have described the form of the three main acoustic mode families present in optomechanical shells, namely the Rayleigh–Lamb waves, longitudinal waves and Love waves. The velocity dispersion of these acoustic modes exhibits a rich behavior, unlike in solid spheres [53] or on planar surfaces. In particular, these modes exhibit deformation at the inner surface of the shell, far away from the optical mode which is confined in the outer $\sim 1\,\mu$m of the shell. As a result of these properties several applications may be enabled.

Specifically, it is proposed [58–60] that a Bose–Einstein condensate (BEC) confined inside an optomechanical resonator may be used to observe state transfer between Schrödinger fields and phonon fields. A second application that can benefit from optical excitation and sensing of mechanical vibration is the detection and weighing of biological and chemical particles in fluid media [61, 62]. For instance, the inner shell surface can be functionalized with antibodies that bind to a bio-particle of interest, changing the effective mass of the acoustic mode when the bio-particle arrives.

Different from other vibrational modes that are commonly used in optomechanics, the acoustic WGMs [32, 53] that are shown here consist of circulating phonons. Such modes are therefore generally referred to as acoustic vortices [63–65]. As they carry angular momentum, the acoustic vortices that we show here can assist in coupling with BEC [66] and superfluid vortices [67–69].

Acknowledgments

This work was supported by the Defense Advanced Research Projects Agency's Optical Radiation Cooling and Heating in Integrated Devices (ORCHID) program through a grant from the Air Force Office of Scientific Research.

References

[1] Carmon T, Rokhsari H, Yang L, Kippenberg T and Vahala K 2005 Temporal behavior of radiation-pressure-induced vibrations of an optical microcavity phonon mode *Phys. Rev. Lett.* **94** 223902

[2] Rokhsari H, Kippenberg T, Carmon T and Vahala K 2005 Radiation-pressure-driven micro-mechanical oscillator *Opt. Express* **13** 5293–301

[3] Kippenberg T J, Rokhsari H, Carmon T, Scherer A and Vahala K J 2005 Analysis of radiation-pressure induced mechanical oscillation of an optical microcavity *Phys. Rev. Lett.* **95** 033901

[4] Povinelli M, Johnson S and Joannopoulos J 2005 Slow-light, band-edge waveguides for tunable time delays *Opt. Express* **13** 7145–59

[5] Arcizet O, Cohadon P-F, Briant T, Pinard M and Heidmann A 2006 Radiation-pressure cooling and optomechanical instability of a micromirror *Nature* **444** 71–4
[6] Gigan S, Bohm H, Paternostro M, Blaser F, Langer G, Hertzberg J, Schwab K, Bauerle D, Aspelmeyer M and Zeilinger A 2006 Self-cooling of a micromirror by radiation pressure *Nature* **444** 67–70
[7] Kleckner D and Bouwmeester D 2006 Sub-Kelvin optical cooling of a micromechanical resonator *Nature* **444** 75–8
[8] Carmon T and Vahala K J 2007 Modal spectroscopy of optoexcited vibrations of a micron-scale on-chip resonator at greater than 1 GHz frequency *Phys. Rev. Lett.* **98** 123901
[9] Metzger C and Karrai K 2004 Cavity cooling of a microlever *Nature* **432** 1002–5
[10] Corbitt T, Ottaway D, Innerhofer E, Pelc J and Mavalvala N 2006 Measurement of radiation-pressure-induced optomechanical dynamics in a suspended Fabry–Perot cavity *Phys. Rev.* A **74** 021802
[11] Metzger C, Ludwig M, Neuenhahn C, Ortlieb A, Favero I, Karrai K and Marquardt F 2008 Self-induced oscillations in an optomechanical system driven by bolometric backaction *Phys. Rev. Lett.* **101** 133903
[12] Okamoto H, Ito D, Onomitsu K, Sanada H, Gotoh H, Sogawa T and Yamaguchi H 2011 Vibration amplification, damping and self-oscillations in micromechanical resonators induced by optomechanical coupling through carrier excitation *Phys. Rev. Lett.* **106** 036801
[13] Tallur S, Sridaran S and Bhave S A 2011 A monolithic radiation-pressure driven, low phase noise silicon nitride opto-mechanical oscillator *Opt. Express* **19** 24522–9
[14] Shen Y R and Bloembergen N 1965 Theory of stimulated Brillouin and Raman scattering *Phys. Rev.* **137** A1787–805
[15] Yariv A 1965 Quantum theory for parametric interactions of light and hypersound *IEEE J. Quantum Electron.* **1** 28–36
[16] Bahl G, Kim K H, Lee W, Liu J, Fan X and Carmon T 2012 Brillouin actuation of microfluidic optomechanical (μFOM) resonators submitted
[17] Chiao R Y, Townes C H and Stoicheff B P 1964 Stimulated Brillouin scattering and coherent generation of intense hypersonic waves *Phys. Rev. Lett.* **12** 592–5
[18] Zel'dovich B Y, Popocivhec V I, Ragul'skii V V and Faisullov F S 1972 Connection between the wave fronts of the reflected and exciting light in stimulated Mandel'shtem–Brillouin scattering *JETP Lett.* **15** 109
[19] Okawachi Y, Bigelow M S, Sharping J E, Zhu Z, Schweinsberg A, Gauthier D J, Boyd R W and Gaeta A L 2005 Tunable all-optical delays via Brillouin slow light in an optical fiber *Phys. Rev. Lett.* **94** 153902
[20] Rich T C and Pinnow D A 1972 Total optical attenuation in bulk fused silica *Appl. Phys. Lett.* **20** 264–6
[21] Lee S A, Lindsay S M, Powell J W, Weidlich T, Tao N J, Lewen G D and Rupprecht A 1987 A Brillouin scattering study of the hydration of Li- and Na-DNA films *Biopolymers* **26** 1637–65
[22] Cheng W, Wang J, Jonas U, Fytas G and Stefanou N 2006 Observation and tuning of hypersonic bandgaps in colloidal crystals *Nature Mater.* **5** 830–6
[23] Zarinetchi F and Smith S 1991 Stimulated Brillouin fiber-optic laser gyroscope *Opt. Lett.* **16** 229–31
[24] Cotter D 1982 Observation of stimulated Brillouin scattering in low-loss silica fibre at 1.3 μm *Electron. Lett.* **18** 495–6
[25] Zhang J-Z and Chang R K 1989 Generation and suppression of stimulated Brillouin scattering in single liquid droplets *J. Opt. Soc. Am.* B **6** 151–3
[26] Kuok M H, Lim H S, Ng S C, Liu N N and Wang Z K 2003 Brillouin study of the quantization of acoustic modes in nanospheres *Phys. Rev. Lett.* **90** 255502
[27] Dainese P, Russell P S J, Joly N, Knight J C, Wiederhecker G S, Fragnito H L, Laude V and Khelif A 2006 Stimulated Brillouin scattering from multi-GHz-guided acoustic phonons in nanostructured photonic crystal fibres *Nature Phys.* **2** 388–92
[28] Grudinin I S, Matsko A B and Maleki L 2009 Brillouin lasing with a CaF_2 whispering gallery mode resonator *Phys. Rev. Lett.* **102** 043902
[29] Tomes M and Carmon T 2009 Photonic micro-electromechanical systems vibrating at X-band (11-GHz) rates *Phys. Rev. Lett.* **102** 113601

[30] Matsko A B, Savchenkov A A, Ilchenko V S, Seidel D and Maleki L 2009 Optomechanics with surface-acoustic-wave whispering-gallery modes *Phys. Rev. Lett.* **103** 257403
[31] Shelby R, Levenson M and Bayer P 1985 Resolved forward Brillouin scattering in optical fibers *Phys. Rev. Lett.* **54** 939–42
[32] Bahl G, Zehnpfennig J, Tomes M and Carmon T 2011 Stimulated optomechanical excitation of surface acoustic waves in a microdevice *Nature Commun.* **2** 403
[33] Savchenkov A A, Matsko A B, Ilchenko V S, Seidel D and Maleki L 2011 Surface acoustic wave opto-mechanical oscillator and frequency comb generator *Opt. Lett.* **36** 3338–40
[34] Bahl G, Tomes M, Marquardt F and Carmon T 2012 Observation of spontaneous Brillouin cooling *Nature Phys.* **8** 203–7
[35] Grudinin I S, Lee H, Painter O and Vahala K J 2010 Phonon laser action in a tunable two-level system *Phys. Rev. Lett.* **104** 083901-4
[36] Tomes M, Marquardt F, Bahl G and Carmon T 2011 Quantum-mechanical theory of optomechanical Brillouin cooling *Phys. Rev.* A **84** 063806
[37] Savchenkov A A, Matsko A B, Ilchenko V S, Strekalov D and Maleki L 2007 Direct observation of stopped light in a whispering-gallery-mode microresonator *Phys. Rev.* A **76** 023816
[38] Carmon T, Schwefel H G L, Yang L, Oxborrow M, Stone A D and Vahala K J 2008 Static envelope patterns in composite resonances generated by level crossing in optical toroidal microcavities *Phys. Rev. Lett.* **100** 103905
[39] Psaltis D, Quake S R and Yang C 2006 Developing optofluidic technology through the fusion of microfluidics and optics *Nature* **442** 381–6
[40] Fan X, White I M, Shopova S I, Zhu H, Suter J D and Sun Y 2008 Sensitive optical biosensors for unlabeled targets: a review *Anal. Chim. Acta* **620** 8–26
[41] Fan X and White I M 2011 Optofluidic microsystems for chemical and biological analysis *Nature Photon.* **5** 591–7
[42] Zhu J, Özdemir Ş K, Xiao Y-F, Li L, He L, Chen D-R and Yang L 2009 On-chip single nanoparticle detection and sizing by mode splitting in an ultrahigh-*Q* microresonator *Nature Photon.* **4** 46–9
[43] Vollmer F and Arnold S 2008 Whispering-gallery-mode biosensing: label-free detection down to single molecules *Nature Methods* **5** 591–6
[44] Vollmer F, Arnold S and Keng D 2008 Single virus detection from the reactive shift of a whispering-gallery mode *Proc. Natl Acad. Sci. USA* **105** 20701–4
[45] Lu T, Lee H, Chen T, Herchak S, Kim J-H, Fraser S E, Flagan R C and Vahala K 2011 High sensitivity nanoparticle detection using optical microcavities *Proc. Natl Acad. Sci. USA* **108** 5976–9
[46] Shopova S I, White I M, Sun Y, Zhu H, Fan X, Frye-Mason G, Thompson A and Ja S-j 2012 On-column micro gas chromatography detection with capillary-based optical ring resonators *Anal. Chem.* **80** 2232–8
[47] Reddy K, Guo Y, Liu J, Lee W, Khaing Oo M K and Fan X 2012 Rapid, sensitive, and multiplexed on-chip optical sensors for micro-gas chromatography *Lab Chip* **12** 901–5
[48] Kim K H, Bahl G, Lee W, Liu J, Tomes M, Fan X and Carmon T 2012 Cavity optomechanics on a microfluidic resonator submitted (arXiv:1205.5477)
[49] Sun Y, Shopova S I, Wu C-S, Arnold S and Fan X 2010 Bioinspired optofluidic FRET lasers via DNA scaffolds *Proc. Natl Acad. Sci. USA* **107** 16039–42
[50] Knight J, Cheung G, Jacques F and Birks T 1997 Phase-matched excitation of whispering-gallery-mode resonances by a fiber taper *Opt. Lett.* **22** 1129–31
[51] Cai M and Vahala K 2001 Highly efficient hybrid fiber taper coupled microsphere laser *Opt. Lett.* **26** 884–6
[52] Oxborrow M 2007 Traceable 2-D Finite-element simulation of the whispering-gallery modes of axisymmetric electromagnetic resonators *IEEE Trans. Microw. Theory Tech.* **55** 1209–18
[53] Zehnpfennig J, Bahl G, Tomes M and Carmon T 2011 Surface optomechanics: calculating optically excited acoustical whispering gallery modes in microspheres *Opt. Express* **19** 14240–8
[54] Tomes M, Marquardt F, Bahl G and Carmon T 2011 Quantum mechanical theory of optomechanical Brillouin cooling *Phys. Rev.* A **84** 063806

[55] Sumetsky M, Dulashko Y and Windeler R S 2010 Optical microbubble resonator *Opt. Lett.* **35** 898–900
[56] Lee W, Sun Y, Li H, Reddy K, Sumetsky M and Fan X 2011 A quasi-droplet optofluidic ring resonator laser using a micro-bubble *Appl. Phys. Lett.* **99** 091102
[57] Berneschi S, Farnesi D, Cosi F, Conti G N, Pelli S, Righini G C and Soria S 2011 High *q* silica microbubble resonators fabricated by arc discharge *Opt. Lett.* **36** 3521–3
[58] Zhang K, Chen W, Bhattacharya M and Meystre P 2010 Hamiltonian chaos in a coupled BEC-optomechanical-cavity system *Phys. Rev.* A **81** 013802
[59] Steinke S K and Meystre P 2011 Role of quantum fluctuations in the optomechanical properties of a Bose–Einstein condensate in a ring cavity *Phys. Rev.* A **84** 023834
[60] Singh S, Jing H, Wright E M and Meystre P 2012 Quantum state transfer between a Bose–Einstein condensate and an optomechanical mirror (arXiv:1202.6100)
[61] Burg T P, Godin M, Knudsen S M, Shen W, Carlson G, Foster J S, Babcock K and Manalis S R 2007 Weighing of biomolecules, single cells and single nanoparticles in fluid *Nature* **446** 1066–9
[62] Barton R A, Ilic B, Verbridge S S, Cipriany B R, Parpia J M and Craighead H G 2010 Fabrication of a nanomechanical mass sensor containing a nanofluidic channel *Nano Lett.* **10** 2058–63
[63] Lugt H J 1983 *Vortex Flow in Nature and Technology* (New York: Wiley-Interscience)
[64] Sathaye A and Lal A 2001 An acoustic vortex generator for microfluidic particle entrapment *Ultrasonics Symp., 2001 IEEE* vol 1, pp 641–4
[65] Dashti P Z, Alhassen F and Lee H P 2006 Observation of orbital angular momentum transfer between acoustic and optical vortices in optical fiber *Phys. Rev. Lett.* **96** 043604
[66] Abo-Shaeer J R, Raman C, Vogels J M and Ketterle W 2001 Observation of vortex lattices in Bose–Einstein condensates *Science* **292** 476–9
[67] Feynman R 1955 Application of quantum mechanics to liquid helium *Progress in Low Temperature Physics* ed C Gorter vol 1 (Amsterdam: Elsevier) pp 17–53
[68] Roberts P H and Donnelly R J 1974 Superfluid mechanics *Annu. Rev. Fluid Mech.* **6** 179–225
[69] Marston P L and Fairbank W M 1977 Evidence of a large superfluid vortex in ^{4}He *Phys. Rev. Lett.* **39** 1208–11